

Article

Manipulation of Laser Distribution to Mitigate the Space-Charge Effect for Improving the Performance of a THz Coherent Undulator Radiation Source

Siriwan Krainara *, Shuya Chatani, Heishun Zen, Toshiteru Kii and Hideaki Ohgaki 

Institute of Advanced Energy, Kyoto University, Gokasho, Uji, Kyoto 611-0011, Japan; chatani.shuuya.22z@st.kyoto-u.ac.jp (S.C.); zen@iae.kyoto-u.ac.jp (H.Z.); kii@iae.kyoto-u.ac.jp (T.K.); ohgaki.hideaki.2w@kyoto-u.ac.jp (H.O.)

* Correspondence: siriwan.krainara.82r@st.kyoto-u.ac.jp; Tel.: +81-809-535-3518

Received: 9 October 2018; Accepted: 5 November 2018; Published: 7 November 2018



Abstract: A THz coherent undulator radiation (THz-CUR) source has been developed at the Institute of Advanced Energy, Kyoto University. A photocathode Radio-Frequency (RF) gun and a bunch compressor chicane are used for generating short-bunch electron beams. When the electron beam energy is low, the space-charge effect strongly degrades the beam quality, such as the bunch length and the energy spread at the high bunch charge condition at around 160 pC, and results in the reduction of the highest frequency and the maximum radiated power of the THz-CUR. To mitigate the space charge effect, we have investigated the dependence of the electron beam quality on the laser distribution in transverse and longitudinal directions by using a numerical simulation code, General Particle Tracer GPT. The manipulation of the laser distribution has potential for improving the performance of the THz-CUR source. The electron bunch was effectively compressed with the chicane magnet when the laser transverse distribution was the truncated Gaussian profile, illuminating a cathode. Moreover, the compressed electron bunch was shortened by enlarging the laser pulse width. Consequently, an enhancement of the radiated power of the THz-CUR has been indicated.

Keywords: coherent undulator radiation (CUR); space charge effect; manipulation of laser distribution; performance

1. Introduction

Recently, thanks to the rapid evolution of ultrashort pulse laser technology based on solid-state lasers, intense THz pulses are now widely available [1–3]. As a consequence, research undertaken to study nonlinear phenomena driven by the intense THz pulses has rapidly evolved [4]. Initially, wideband THz pulses can be generated by the rectification of ultrashort near-infrared laser pulses [5]. Compared to the wideband sources, narrowband intense THz pulses are more suitable to study the more detailed process, which has a sharp resonance at the certain frequency. Some researchers developed multicycle quasi-monochromatic THz sources based on the ultrashort-pulse near-infrared lasers [6]. On the other hand, the accelerator-based THz sources such as free electron lasers (FELs) [7,8], which can generate intense quasi-monochromatic THz pulses, are also good candidates to be used for nonlinear THz spectroscopy. In addition to FELs, nowadays, coherent radiations directly generated from an ultrashort high-energy electron bunch are attracting interest for their potential to generate intense quasi-monochromatic THz pulses via coherent undulator radiation (CUR) source and superradiance THz FELs [9,10]. They could possibly generate megawatt (MW)-class quasi-monochromatic THz pulses. At the Institute of Advanced Energy, Kyoto University, a compact THz-CUR source has been developed to provide such MW-class quasi-monochromatic THz pulses [11].

The main goal of this system is to produce intense quasi-monochromatic THz-CUR radiations, which cover the wavelength and the frequency range from 350 to 1750 μm and 0.17 to 0.9 THz, respectively, with the electron beam energy of 4.6 MeV. This frequency range is particularly interesting for study of the vibration of molecules or rotation of spin, such as of biological molecules or magnetic materials [12–14].

In the compact accelerator system, a photocathode RF gun used as an electron source can provide an electron beam with a high charge. The electrons are generated by photoemission by injecting a UV laser with a wavelength of 266 nm to a cathode. The laser pulse duration was measured as 5.8 ± 0.2 ps in Full-Width-Half-Maximum (FWHM) with Gaussian distribution [15]. The transverse laser size was measured at the cathode surface of 0.5 mm in root-mean-square (rms) with Gaussian spatial distribution. An electron bunch with the beam energy of 4.6 MeV was compressed by a bunch compressor chicane before passing through a planar undulator to generate an intense quasi-monochromatic THz-CUR. An electron bunch length must be shorter than the radiation wavelength to create coherent radiations. The power of the coherent radiation increases with the square of the number of radiating electrons per bunch, N^2 . The schematic of the THz-CUR system is shown in Figure 1. According to the observations [16,17], the THz-CUR energy obviously was saturated at the high bunch charge region because the radiated energy was affected by the influence of the space-charge forces in a short electron bunch, which resulted in the bunch lengthening and degradation of the electron beam quality. At present, the frequency of THz-CUR can be tuned in the range of 0.16–0.65 THz with the bunch charge of 60 pC. However, when we increase the bunch charge to be 160 pC, the THz-CUR at 0.65 THz cannot be generated. The measured results of total radiated energy and the peak power in a micropulse at 0.16 THz were approximately 1 μJ and 20 kW with the bunch charge of 160 pC, respectively. We found that the bunch length estimated by using coherent transition radiation (CTR) had the duration of 1.43 ps-FWHM and 1.81 ps-FWHM with the bunch charge of 60 pC and 160 pC, respectively [18].

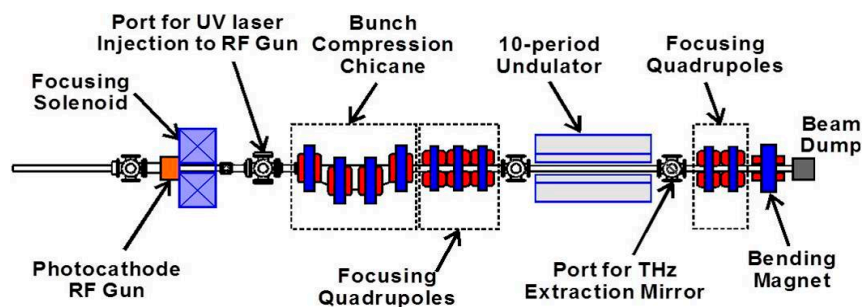


Figure 1. Diagram of the THz-coherent undulator radiation (CUR) system at Kyoto University.

The photocathode electrons have been used in many facilities, such as free electron laser (FEL) sources, for producing short bunch length with high charge [19–22]. However, a problem of the high space-charge effect in the low-energy region is causing emittance blow-up. The electron beam emittance has been minimized as much as possible in order to reach the higher power. Therefore, to keep the emittance low, the space-charge effect must be substantially mitigated. The technique of shaping the laser distribution in order to reduce the space-charge effect causing emittance has been reported in many studies [23–26]. The drive laser pulse must be expanded or made uniform before illuminating the cathode to generate the best emittance of the electron beam. Moreover, in Ref. [27], it was reported that the transverse emittance at the Linac Coherent Light Source (LCLS) injector was reduced with applying the truncated Gaussian profile, which can be done simply by clipping using an aperture [28]. The space-charge force is more linear and can be compensated by applying a solenoid field. If the space-charge effect is not eliminated, it can disturb the electron bunch along the beam transportation [29]. Accordingly, this method could be used to control the electron bunch or the energy

chirp before bunch compression, which is deformed by the space-charge effect. With the reduction of this effect, the energy chirp would be suitable and could be successfully performed for bunch compression to obtain a short bunch length.

In this paper, the main purpose is to find a way to mitigate the space-charge effect. An increase of electron beam energy can reduce the space-charge force and be helpful to enhance the radiated power. However, our source has a limitation of RF power, and also the THz-CUR project is targeting a compact system, so using an additional acceleration tube cannot be an acceptable means of increasing the electron energy. Therefore, to eliminate the problem addressed above, it is necessary to study how the laser shape is significant for the bunch compression and the impact on obtaining the short bunch length and high radiated power. Section 2 demonstrates clearly how the space-charge effect impacts the electron beam quality and exhibits the process of bunch compression. For a better understanding, the dependence of the electron beam quality on the operating conditions, such as the parameters of the laser, including laser pulse width and transverse size, have been investigated and are shown in Section 3. The manipulation of the laser distribution is presented as a powerful tool to optimize the photoinjector performance. Section 4 is dedicated to the results of compressed bunch length, radiated power, and the improvement in THz-CUR source performance after manipulating the laser distributions. Finally, in Section 5, we make conclusions on the results.

2. Space-Charge Effect

Although a high bunch charge can be produced from the photocathode, an emission of electrons is affected by interacting with a self-field at the cathode surface. Each electron interacts inside the bunch with each other one and is also subject to the electric and magnetic fields generated from all the other electrons in the bunch. Therefore, the space-charge effect occurs to a great degree in a short electron bunch with high bunch charge and scales as $1/\gamma^2$ [30–32]. It is the main factor causing degradation of electron beam quality in a low-energy source, therefore the electron bunch can easily be distorted by this force. The investigation of the longitudinal phase space is presented as follows.

2.1. Longitudinal Phase Space before Compression

In order to get a suitable energy chirp, the longitudinal phase space was optimized with the RF phase and the solenoid field. The optimization is to obtain a small emittance in both planes at RF gun exit and to preserve a linear energy chirp for the bunch compression in a chicane. In order to understand the electron beam behavior with the space-charge effect, Figure 2 shows the longitudinal particle distribution at the chicane entrance comparing between turning off and turning on the space-charge effect from general particle tracer (GPT) simulation [33] with the present laser distribution of our THz-CUR source. Although the solenoid focusing can be used especially for the compensation of the linear space-charge force, it cannot be used for the nonlinear space-charge force on the cathode surface.

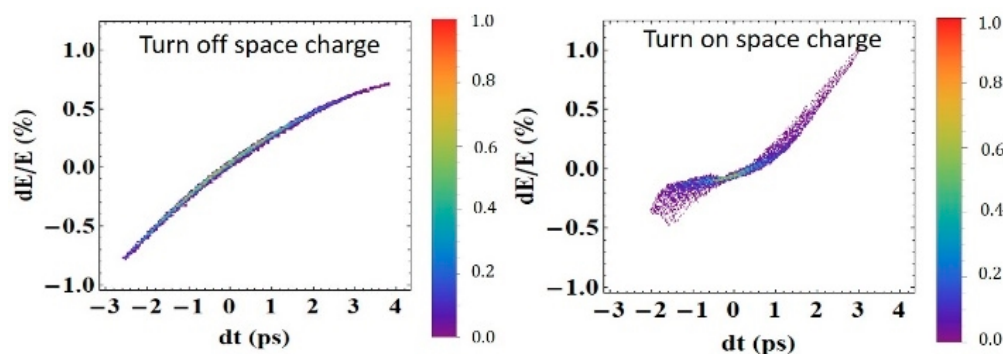


Figure 2. Longitudinal distribution at the chicane entrance in the case of turning off and turning on the space-charge effect at 60 pC charge.

Figure 3a shows the longitudinal phase space distribution at different bunch charges given by GPT simulation at the chicane entrance in order to check the influence of the nonlinear space-charge force on an electron bunch. Although the laser injection phase and the solenoid field have been set to the optimum point for finding the suitable energy chirp before the compression process, the distortion of the electron bunch occurs due to the space-charge force or the charge repulsion force. It was found that the bunch’s energy chirp decreased with the increase of the bunch charge owing to the large space-charge force. The bunch’s tail loses energy while the head gains energy to decrease the energy chirp, which is required for the bunch compression. In the transverse space, the coupling effect between the transverse and longitudinal emittance directly leads to the evolution of particle distribution to disturb the energy chirp and results in bunch lengthening. The perturbation of bunch length caused by the beam divergence at the gun exit can be simply described by Equation (1) [34,35]:

$$\Delta\sigma_z = \frac{L}{2}(x'^2 + y'^2) \tag{1}$$

where L is the distance of the drift space and x' and y' are the beam divergence in the horizontal and vertical planes, respectively. In general, the emittance blow-up at higher bunch charge leads to the increase of bunch length, according to Equation (1). Therefore, the effect of beam divergence is one of the factors preventing the generation of a short electron bunch at low energy. Reducing the beam divergence is a powerful process to prepare the chirp for compressing the electron bunch, which can be obtained by the manipulation of the laser distribution.

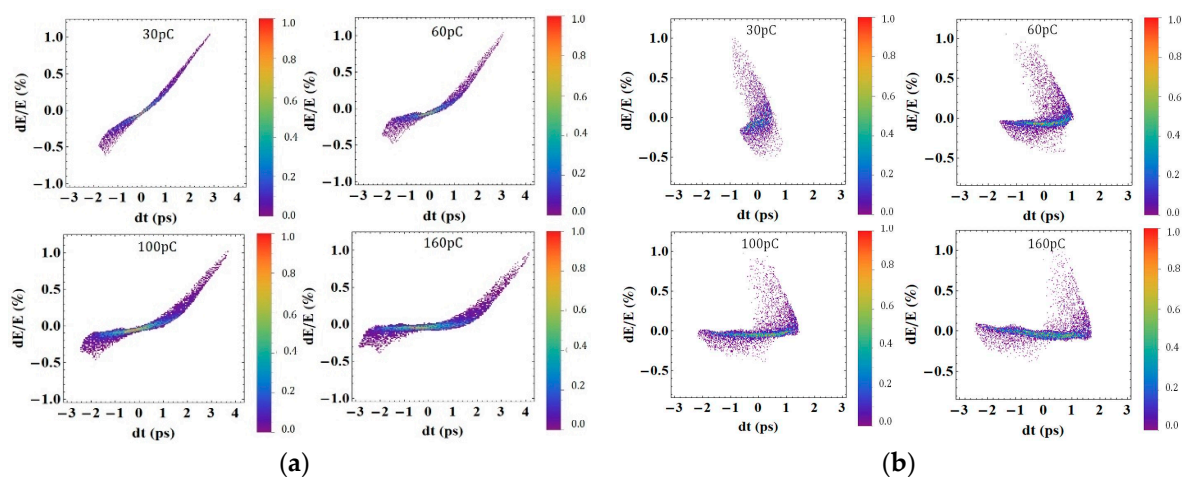


Figure 3. Energy–time phase space with turning on the space-charge effect with the bunch charge of 30 pC, 60 pC, 100 pC, and 160 pC (a) before and (b) after the bunch compression chicane if the cathode is excited by a laser pulse width of 5.8 ps-FWHM and Gaussian profile.

2.2. Bunch Compression with Negative R_{56} Chicane

In the general approach to bunch compression, the first-order momentum compaction R_{56} has to match with the bunch’s energy chirp, h by $R_{56} = -1/h$. The energy chirp is defined by the slope of the energy spread (dE) over the electron position (dt), $h = dE/cdt$. Our chicane bunch compressor was designed to compress a bunch with a negative linear longitudinal dispersion ($R_{56} < 0$) and, thus, a positive energy chirp ($h > 0$). The energy chirp of this machine is mainly induced by the laser injection phase, which is determined by the acceleration efficiency of the electron beam. The diagram of the bunch compression chicane and the evolution of the longitudinal phase space are presented in Figure 4. The tail of the bunch with higher energy passes through the chicane with a shorter path length compared to the head with lower energy. When the electron bunch disturbed by the space-charge effect passes through the dispersive section of the bunch compressor, the electron beam quality is extremely

degraded, resulting in the diminishment of an effective bunch compression [36]. The evolution of longitudinal phase space or the change in bunch length after bunch compression can be determined by Equation (2) [37,38]:

$$\sigma_{zf} = \sigma_{zi} + R_{56}\delta E + T_{566}\delta E^2 + U_{5666}\delta E^3 + f(T_{511}, \dots, T_{565}) \tag{2}$$

where σ_{zi} and σ_{zf} are the bunch length before and after compression, respectively; the coefficients of the momentum compaction factor are in terms of R_{56} , T_{566} , and U_{5666} ; and δE is energy spread. The higher-order terms of T_{566} and U_{5666} can be simply defined as $-3R_{56}/2$ and $2R_{56}$, respectively. The energy chirp must be positive or the R_{56} should be negative so as to shorten the bunch length. However, the bunch lengthening is also caused by the beam divergence, which largely depends on the second-order effects, $f(T_{511}, \dots, T_{565})$ consisting of the transfer matrix coefficients from T_{511} to T_{565} , which can be explained as $T_{511}\sigma_x^2$, $T_{512}\sigma_x\sigma_{x'}$, $T_{522}\sigma_{x'}^2$, $T_{533}\sigma_y^2$, $T_{534}\sigma_y\sigma_{y'}$, and $T_{544}\sigma_{y'}^2$. The terms σ_x and σ_y are referred to as the electron beam size in the horizontal and vertical planes, respectively, within a standard deviation by assuming its Gaussian distribution, and the transverse divergences are defined in terms of $\sigma_{x'}$ and $\sigma_{y'}$. The increase of the bunch length can be affected by the emittance blow-up due to the space-charge effect, since the parameters of beam size and transverse divergence are linked to the transverse emittance.

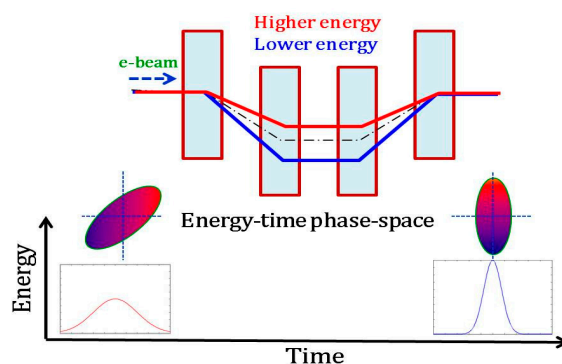


Figure 4. Magnet arrangement in the magnetic chicane and the evolution of energy-time phase space during passing through the chicane.

According to the optimization of the machine conditions of 5.8 ps-FWHM and Gaussian profile, we scanned the machine parameters, such as the RF phase, solenoid field, and chicane field. The method used for optimization was to calculate the space-charge factor [26] as the functions of the RF phase and solenoid field, and then to consider a suitable energy chirp for compression, which would be close to the value of the energy chirp in the case of no space charge. It was found that the optimal RF phases would be 20 and 10.5 degrees, and the solenoid fields were optimal at 0.162 and 0.103 Tesla to provide a suitable energy chirp for the bunch compression at the bunch charge of 160 pC in the cases of turning off and turning on the space-charge effect, respectively. Obviously, the longitudinal particle distributions are not completely rotated after passing through the chicane magnet, even with careful adjustment to find the optimum chicane magnetic field (Figure 3b), so it should be of concern. The details of optimization are in preparation and will be reported elsewhere [39]. As explained above in the introduction, the emittance blow-up or the beam divergence is gradually expanded on account of the space-charge effect causing the rotation of the longitudinal phase space and disturbing the electron bunch. This effect can be minimized by shaping the laser distribution both in transverse and longitudinal directions. Therefore, the degradation of electron beam quality, such as via bunch lengthening due to the nonlinear space-charge force disturbing the electron bunch, can be mitigated by the manipulation of the laser distribution applied in our source.

3. Manipulation of Laser Distribution

To intentionally restrain the space-charge effect, the manipulation of the drive laser pulse both in the transverse and longitudinal directions before injecting the cathode is required for producing the short electron bunch length. This can help to reduce the longitudinal emittance due to the higher-order effects and also to avoid inducing the increase of the bunch length [37]. An analytical model of the Gaussian beam to express the charge density (ρ) referring to the space-charge force can be written as the following equation [40]:

$$\rho = \frac{Q}{(2\pi)^{3/2}\sigma_x^2 \text{Erf}\left(\frac{r_a}{\sqrt{2}\sigma_x}\right)^2 \sigma_z} e^{-((x^2+y^2)/2\sigma_x^2)-(z^2/2\sigma_z^2)} \tag{3}$$

where Q is the total charge, Erf is an error function, σ_x and σ_z are the rms beam sizes in the transverse and longitudinal directions, respectively, and r_a is the aperture radius. This equation clearly shows that the charge density depends on the bunch charge (in both planes), which can be controlled by the injection laser in a photocathode RF gun for $x^2 + y^2 < r_a^2$. The charge density is equal to zero ($\rho = 0$) if $x^2 + y^2 > r_a^2$, where the spatial distributions in the x and y planes are determined as Gaussian distributions.

In this study, we have investigated the electron beam quality at the difference of transverse laser distribution between Gaussian and truncated Gaussian profiles, and have also studied the dependence of the compressed bunch length on the laser pulse width. The laser parameters used are listed in Table 1. The laser distributions illuminating the cathode are examined in both the transverse and longitudinal directions as follows:

1. Transverse laser profile: The transverse truncated Gaussian profile can be modified by clipping the drive laser of the Gaussian profile with an aperture before irradiation. The laser spatial distribution has to be cut at the center, as shown in Figure 5a.

Table 1. Distributions of a laser illuminating the cathode with the bunch charge of 160 pC and 300 pC.

Transverse Laser Size of 0.5 mm-rms	Laser Pulse Width FWHM
Gaussian	5.8 ps, 10 ps, 15 ps, 20 ps
truncated Gaussian	5.8 ps, 10 ps, 15 ps, 20 ps

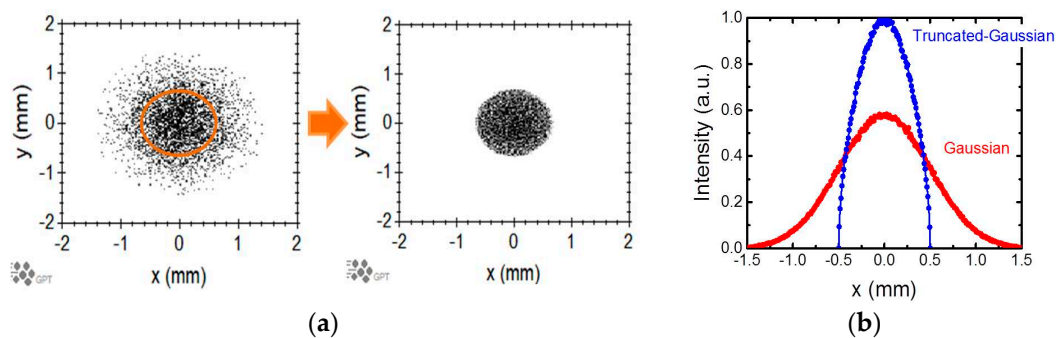


Figure 5. (a) Transverse laser profile: (left) Gaussian and (right) truncated Gaussian clipped with aperture size of 0.5 mm; and (b) laser distribution for the transverse profile before injecting the cathode.

Normally, the emittance blow-up due to the linear space-charge effect could be compensated by the solenoid field. In order to mitigate the nonlinear space-charge effect, the ratio between the beam size and aperture size (σ_x/r_a) should be the factor of 1 to obtain a linear space-charge force. That means the laser profile should be truncated at 0.5 mm whenever the radius of spatial distribution is $\sigma_x = 0.5$ mm in the Gaussian distribution. The truncated Gaussian profile has a more linear space-charge force in

comparison to the Gaussian profile in the transverse direction [27]. The optimization of the transverse laser size is to correct the radial RF field effects and the nonlinear space-charge effect [41]. The emittance has been investigated versus the aperture size, as plotted in Figure 6. To achieve a reasonable aperture size for this condition, the spatial distribution has to be clipped by using the aperture radius of 0.5 mm. The transverse emittance was compensated and minimized from 2.6 to 1.2 mm-mrad. The measured result in Ref. [27] reported that the quality of the electron beam (emittance) was successfully improved with the truncated Gaussian profile. Reducing the aperture size also makes the result of longitudinal emittance gradually decrease as well. An electron beam with low transverse emittance and low longitudinal emittance impacts the bunch compression to attain a short electron bunch.

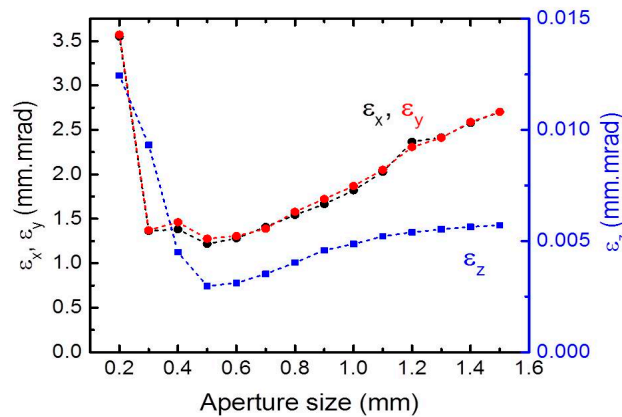


Figure 6. Transverse and longitudinal emittances at different transverse sizes at the entrance of bunch compression with the bunch charge of 160 pC and the laser pulse width of 5.8 ps-FWHM.

2. Laser pulse width: The laser pulse width was enlarged from 5.8 ps-FWHM to 10 ps-FWHM, 15 ps-FWHM, and 20 ps-FWHM with Gaussian distribution as plotted in Figure 7. Since the laser pulse width can be defined as the initial length of the electron bunch, the longitudinal bunch can be deformed more easily by the shorter bunch length owing to a stronger space-charge effect in the longitudinal direction. Due to the charge density of the electron bunch also being determined by the laser pulse width on the cathode, the expanding of the pulse width would have a low effect on electron beam dynamics as well. In practice, the longer laser pulse width can be provided by using the pulse stacking system reported in Ref. [26].

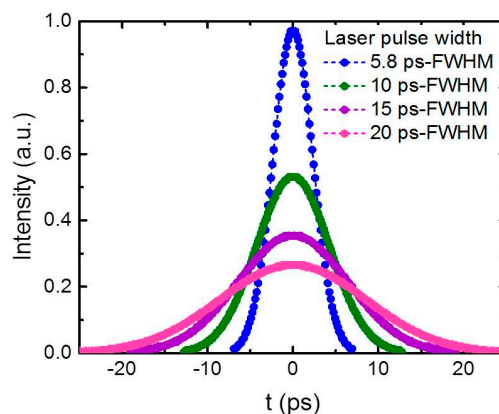


Figure 7. Dependence of the longitudinal electron distribution on the laser pulse width before irradiation with a fixed bunch charge.

Figure 8 clearly presents the longitudinal phase space simulated using the truncated Gaussian profile with the pulse width of 5.8 ps-FWHM and 10 ps-FWHM in the case of the bunch charges of 160 pC

and 300 pC. It is interesting to note that the space-charge force using the laser profile of truncated Gaussian distribution may be more linear and smaller than that of the Gaussian profile. As we know, the reduction of the nonlinear space-charge effect is not only dependent on the laser transverse profile, but also gets lower with a longer laser pulse width. The longitudinal phase space seems almost similar to the case of space-charge effect turn-off (Figure 2).

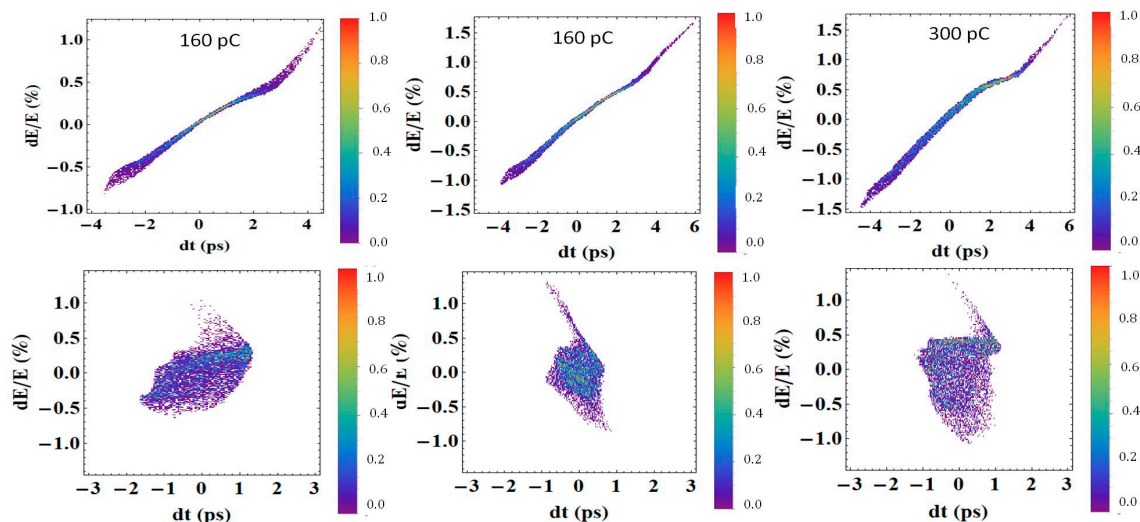


Figure 8. Longitudinal phase space of the electron bunch at the entrance (**top**) and the exit (**bottom**) of the chicane magnet, with truncated Gaussian distribution with the laser pulse width of (**left**) 5.8 ps-FWHM, 160 pC; (**middle**) 10 ps-FWHM, 160 pC; and (**right**) 10 ps-FWHM, 300 pC.

4. Results and Discussion

4.1. Longitudinal Particle Distribution

According to manipulations of the laser distribution before irradiating the cathode to reduce the space-charge effect, it was found that the longitudinal phase space at the entrance of the chicane seems more linear and has a high chirp of energy–time, as shown in Figure 8. Due to a good behavior in the longitudinal phase space, the electron bunch can be compressed to reach a higher peak current after passing through the chicane magnet. The effective bunch compression can be investigated from the peak current and the longitudinal particle distribution. Figure 9 illustrates the longitudinal particle distribution versus peak current in a variety of laser pulse widths. Obviously, the longitudinal particle distribution with high peak current and narrow distribution can be obtained when increasing the laser pulse width. This result clearly shows that the space-charge effect deforming the electron bunch can be considerably lessened with expanding the laser pulse width together with using the truncated Gaussian profile.

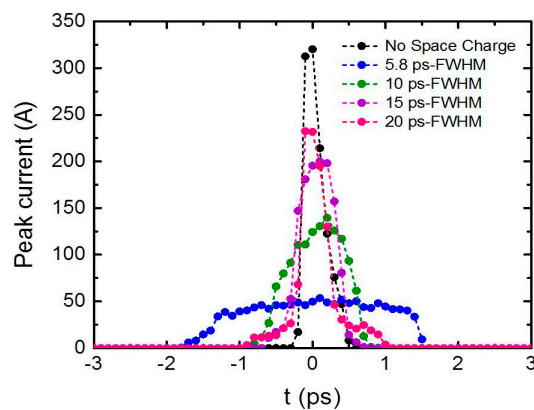


Figure 9. Longitudinal particle distribution after bunch compression for the different laser pulse widths with the truncated Gaussian profile ($r_a = 0.5$ mm) in the case of the bunch charge of 160 pC.

4.2. Electron Bunch Length

From the longitudinal phase space after compression, it was found that the electron bunch can be compressed to achieve a shorter length and a higher peak current by using the long laser pulse width and truncated Gaussian profile. In order to estimate the bunch length, the longitudinal particle distribution as plotted in Figure 9 was converted to the bunch form factor by using a fast Fourier transform (FFT) calculation with high frequency resolution, and was fitted with a function of a bunch form factor with Gaussian distribution ($B_f(\omega, \sigma_z) = \exp(-\omega^2 \sigma_z^2)$). Figure 10 shows the decreases of the simulated bunch length from 1.72 ps to 1.45 ps when keeping the charge constant at 160 pC. By expanding the laser pulse width from 5.8 ps-FWHM to 10 ps-FWHM, the electron bunch was compressed to 0.82 ps-FWHM with using the truncated Gaussian profile, and by enlarging the laser pulse width to 20 ps-FWHM, the compressed electron bunch was shorter than 0.5 ps-FWHM. The space-charge force is more linear when using the truncated Gaussian distribution and the long laser pulse width. It is worth noting that the length of the electron bunch can be compressed to 0.21 ps-FWHM in the case of turning off the space-charge effect with the present laser distribution used in the THz-CUR source. This result would suggest that this is the minimum bunch length available in this source. In order to respond to the requirement of the enhancement of the radiated power in MW-class quasi-monochromatic THz pulses, we have also studied the compression of the electron bunch in the case of increasing the bunch charge to 300 pC. However, the space-charge force is proportional to electron charge, so this force affecting the electron bunch is certainly higher than that with the bunch charge of 160 pC. The compressed result of bunch length at different laser distributions is shown in Figure 10. It can be seen that with the 5.8 ps-FWHM laser pulse width, the electron bunch was not successfully compressed, even when using the truncated Gaussian distribution. The space-charge effect still greatly disturbs the electron bunch. However, the length of the compressed electron bunch was gradually shortened compared to when expanding the laser pulse width.

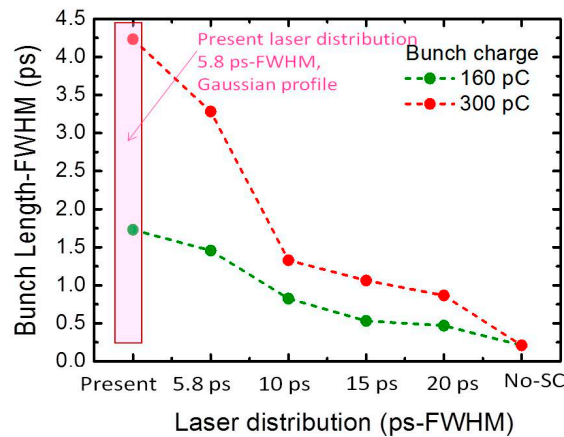


Figure 10. Comparison of the bunch length with the present laser distribution (5.8 ps-FWHM, Gaussian profile) and the laser pulse width of 5.8 ps-FWHM, 10 ps-FWHM, 15 ps-FWHM, and 20 ps-FWHM with a truncated Gaussian profile, and no space-charge effect at the bunch charge of 160 pC and 300 pC.

4.3. Improvement of the THz-CUR Performance

Since the influence of the space-charge force in the short electron bunch affects radiation properties, the improvement of the THz-CUR source performance can be confirmed by calculation of the radiated power. The radiation peak power can be expressed by dividing the radiation energy by the radiation pulse width, $N_u \lambda_r / c$. The energy spectral density for the CUR [42,43] is given by

$$\frac{d^2W}{d\omega d\varphi} = \frac{Q^2 N_u^2 \gamma^2}{4\pi\epsilon_0 hc} \frac{K^2}{(1 + K^2/2)^2} \sum_{m=1}^{\infty} n^2 \left\{ \frac{\sin \left[N_u \pi \left(\frac{\omega}{\omega_r} - 1 \right) \right]}{N_u \pi \left(\frac{\omega}{\omega_r} - 1 \right)} \right\}^2 J^2 \times B_f^2(\omega) \quad (4)$$

where Q is the bunch charge, N_u is the number of undulator periods, γ is the Lorentz factor for the electron, c is the speed of light, ϵ_0 is the permittivity of free space, K is the undulator parameter ($K = 0.934 B_0 [T] \lambda_u [cm]$), JJ is the Bessel function, and $B_f(\omega, \sigma_z)$ is the bunch form factor. The bunch form factor from the longitudinal particle distribution can be expressed as follows:

$$B_f(\omega) = \frac{\sum_{m=1}^N e^{j\omega t_i}}{N} \quad (5)$$

Here, N is the total number of particles and t_i is the temporal location of the i th electron.

The radiated power generated from our source can be calculated from Equation (4) with the 4.6 MeV electron beam and the peak undulator field (B_0) of 0.43 Tesla with 10 periods. Figure 11a illustrates the dependence of the bunch form factor taken from the longitudinal particle distribution on the laser pulse width and transverse profile. The radiated power is proportional to the bunch form factor given by Equation (5), and it can be given by integrating the energy spectral density over the frequency, ω , and the solid angle, φ ($d\varphi \sim \pi / \gamma^2$), and by dividing by the radiation pulse width ($N_u \lambda_r / c$). The spectral bandwidth of the CUR radiation ($\Delta\omega / \omega_0$) is about 10%, as calculated from $1/N_u$. As shown in Figure 11b, the radiated power increased by 127%, 338%, 369%, and 373% with the transverse profile of truncated Gaussian distribution and the longitudinal laser distributions at 5.8 ps-FWHM, 10 ps-FWHM, 15 ps-FWHM, and 20 ps-FWHM, respectively. The radiated power raised up to 385% by turning off the space-charge effect. All cases were compared with the power result calculated from the bunch length with the laser pulse width of 5.8 ps-FWHM and the Gaussian transverse profile. The radiated power with a quasi-monochromatic spectrum at 0.16 THz can be distinguished when using the laser pulse width longer than 10 ps-FWHM. The manipulation of the

laser distribution is helpful in enhancing the form factor and the CUR power because the space-charge effect could be reduced and thus could not substantially disturb the electron bunch compression.

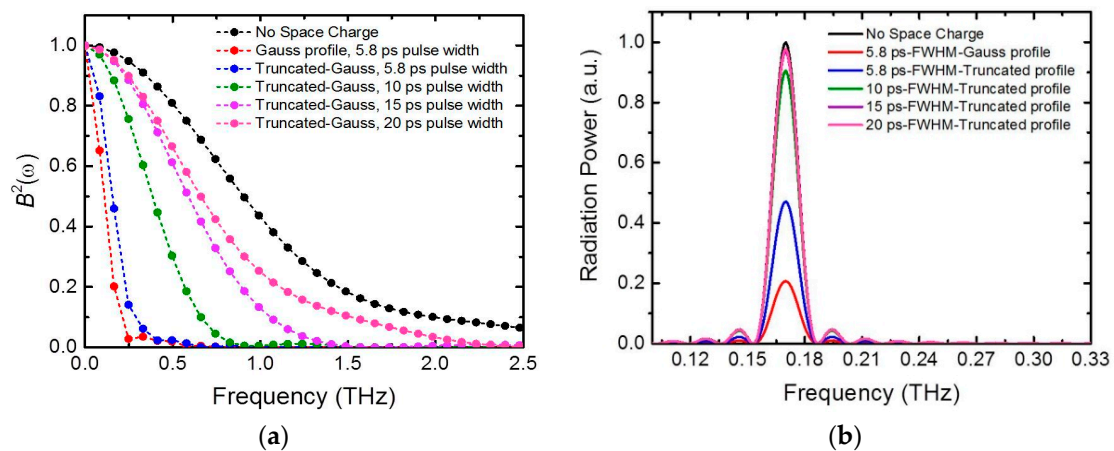


Figure 11. (a) Variations in the bunch form factor as a function of the radiation frequency at the different laser pulse widths simulated by General Particle Tracer (GPT) code, and (b) radiation power spectrum at the different laser pulse widths with bunch charge of 160 pC at 0.16 THz and electron energy of 4.6 MeV.

The radiated power using the laser distribution of 5.8 ps-FWHM pulse width and the truncated Gaussian profile is 2.27-fold higher than that when using the Gaussian distribution. The result of using the truncated Gaussian distribution indicates that the compressed electron bunch is shorter and results in higher radiated power than that when using the Gaussian profile. In the experiment, the radiation pulse energy was measured as a function of the bunch charge, as shown with red dots in Figure 12a. Despite the saturation of radiation energy, the CUR was still generated with the pulse energy of 1.2 μJ with the bunch charge of 160 pC. By applying the truncated Gaussian profile, the radiation energy is expected to increase from 1.2 μJ to 2.7 μJ , as presented in a blue dot. The radiation energy based on measurement is summarized in Table 2. The result is in good agreement with the quadratic function of radiation energy versus the bunch charge ($E \propto Q^2 B_f(\omega)$) to meet the theory of the generation of the CUR. Therefore, the saturation problem of the radiation energy could be solved by using the truncated Gaussian profile. As shown in Figure 12b, enough CUR power at 0.65 THz is successfully generated by using the laser pulse width longer than 10 ps-FWHM. Eventually, the generation of the CUR could be obtained with a wider range of frequencies and also higher radiated power than that from the current experiment.

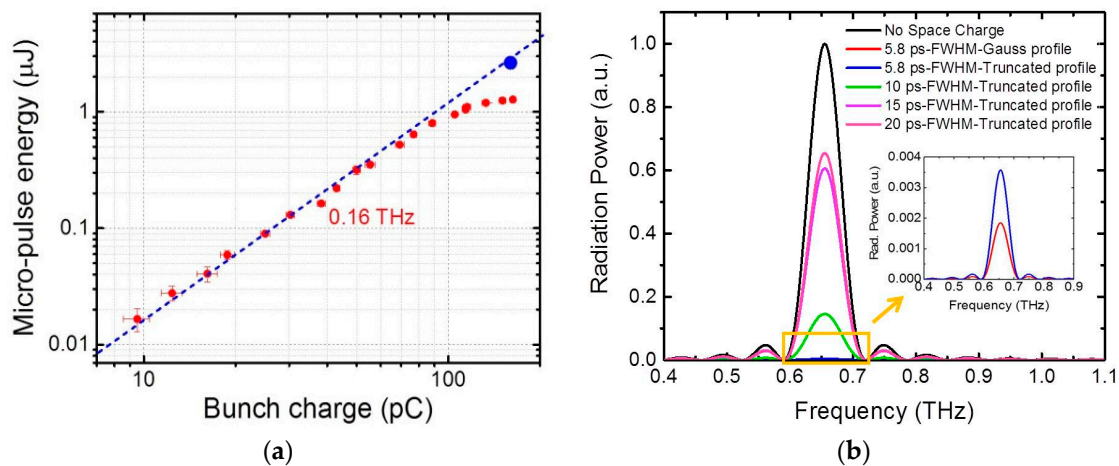


Figure 12. (a) Improvement of the saturation of radiation energy at the frequency of 0.16 THz. The red dots are the measured results, and a blue dot is an estimate of the radiation energy for applying a truncated Gaussian profile; (b) calculated radiation power spectrum with bunch charge of 160 pC at 0.65 THz with different laser distributions.

Table 2. Summary of radiation properties with the bunch charge of 160 pC at the frequency of 0.16 THz.

Laser Distribution	Spatial Distribution	Radiation Energy (μJ)	Peak Power (kW)
5.8 ps-FWHM	Gaussian	1.2 μJ (measured)	20 kW (measured)
5.8 ps-FWHM	Truncated Gaussian	2.7 μJ	45 kW
10 ps-FWHM	Truncated Gaussian	5.2 μJ	87 kW
15 ps-FWHM	Truncated Gaussian	5.6 μJ	94 kW
20 ps-FWHM	Truncated Gaussian	5.7 μJ	95 kW
Turn off the space-charge effect		5.8 μJ	97 kW

4.4. Expected Radiation Power of the THz-CUR at 0.16 THz

According to the result from the experiment, the THz radiation with the bunch charge of 160 pC from our source can be generated with the peak power of 20 kW at 0.16 THz using the laser parameters of 5.8 ps-FWHM and the Gaussian profile. The expected radiation power ($P \propto Q^2 B_f(\omega)$) is estimated from the measured peak power, with the simulated results of the bunch form factor plotted in Figure 11. Figure 13 shows the result of using of the laser pulse width of 10 ps-FWHM with the transverse truncated Gaussian profile; the peak power based on the measurement increased greatly up to about 87 kW and 250 kW with the bunch charge of 160 pC and 300 pC, respectively. The result supports the idea of the mitigation of the space-charge effect for achieving an efficient bunch compression to successfully compress the short electron bunch. The length of the electron bunch impacts on the bunch form factor and corresponds to the generation of high radiation power for the THz-CUR system at Kyoto University. From this result, we can confirm that the THz-CUR can be generated with the peak power of several hundred kW with the bunch charge of 300 pC. Since our source can generate the bunch charge of up to 1000 pC [44], our THz-CUR source will possibly produce the radiation of MW peak power by increasing the bunch charge and reducing the effect disturbing the electron bunch. Moreover, the increase of the electron beam energy will contribute to increasing the radiation power and also mitigating the space-charge effect.

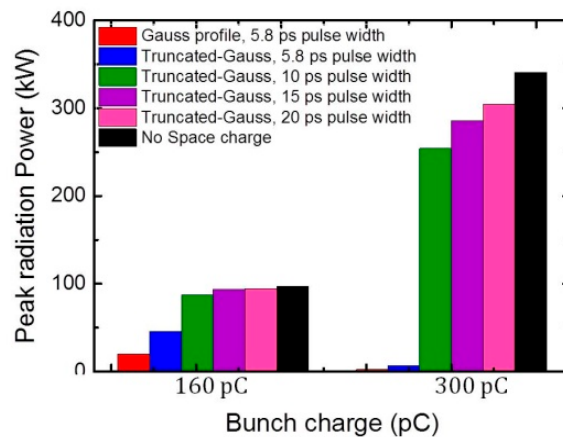


Figure 13. Expected radiation peak power at the fundamental frequency of 0.16 THz with the bunch charge of 160 pC and 300 pC at the THz-CUR source.

5. Conclusions

In this study, we have investigated bunch length as a function of the parameters of the laser, including the pulse width and the transverse distribution, by using the numerical simulation code GPT for mitigating the space-charge effect in a THz-CUR system. It was found that the most powerful way to mitigate the space-charge effect in the THz-CUR system at Kyoto University was to manipulate the laser distribution both in the transverse and longitudinal planes for preventing the degradation of electron beam quality. The high efficiency of chicane bunch compression can be achieved by controlling the transverse laser profile on the cathode with the truncated Gaussian distribution. However, increasing the laser pulse width can obtain the shortening of the length of the compressed electron bunch and also obtain the higher bunch form factor. The generated radiation power of the CUR at 0.16 THz with 160 pC bunch charge increases by 127% and more than 300% by enlarging the laser pulse width to larger than 10 ps-FWHM. The laser distributions of 10 ps-FWHM and the truncated Gaussian profile would be used to solve the problems of the saturation of the pulse energy and the disappearance of the CUR power spectrum in the high-frequency region. The peak radiated power at 0.16 THz could be more than 250 kW. The CUR radiation in the frequency range higher than 0.65 THz with high radiated power would be generated as well. In order to achieve a MW-class radiation source, our THz-CUR source may be able to generate the radiation of MW peak power by increasing the bunch charge and the electron beam energy. The examination of the transverse truncated Gaussian distribution, as well as the enlargement of the laser pulse width to generate the higher radiated power of THz-CUR, will be performed experimentally. In future work, a laser pulse stacking system will be implemented for providing longer laser pulses before illuminating the cathode.

Author Contributions: S.K. conceived the physics concept and method, performed the experiment, simulation, and calculation, and analyzed the results; S.C. performed the simulation and designed the laser pulse stacking system for enlarging the laser pulse width; H.Z. supervised the experiment, advised the simulation, and discussed the results. This research was carried out under the supervision of T.K. and H.O. and S.K. wrote the paper.

Funding: This research was funded by the Japan Society for the Promotion of Science, KAKENHI 26706026.

Conflicts of Interest: The authors declare no conflict of interest.

References

1. Dhillon, S.S.; Vitiello, M.S.; Linfield, E.H.; Davies, A.G.; Hoffmann, M.C.; Booske, J.; Paoloni, C.; Gensch, M.; Weightman, P.; Williams, G.P. The 2017 terahertz science and technology roadmap. *J. Phys. D Appl. Phys.* **2017**, *50*, 043001. [\[CrossRef\]](#)
2. Davies, A.G.; Linfield, E.H.; Johnston, M.B. The development of terahertz sources and their applications. *Phys. Med. Biol.* **2002**, *47*, 3679–3689. [\[CrossRef\]](#) [\[PubMed\]](#)

3. Hafez, H.A.; Chai, X.; Ibrahim, A.; Monda, S.; Férachou, D.; Ropagno, X.; Ozaki, T. Intense terahertz radiation and their applications. *J. Opt.* **2016**, *18*, 093004. [[CrossRef](#)]
4. Tanaka, K.; Hirori, H.; Nagai, M. THz Nonlinear spectroscopy of solids. *IEEE Trans. Terahertz Sci. Technol.* **2011**, *1*, 301–312. [[CrossRef](#)]
5. Vicario, C.; Ovchinnikov, A.O.; Chefanov, O.V.; Hauri, C.P. Multi-Octave Spectrally Tunable Strong-Field Terahertz Laser. 2016. Available online: <https://arxiv.org/abs/1608.05319> (accessed on 4 October 2018).
6. Minamide, H. Development of high-power terahertz-wave sources for finding novel applications. *IEEE Trans. Terahertz Sci. Technol.* **2015**, *5*, 1104–1109.
7. Krishnagopal, S.; Kumar, V.; Maiti, S.; Prabhu, S.S.; Sarkar, S.K. Free electron laser. *Curr. Sci.* **2004**, *87*, 1066–1078. [[CrossRef](#)]
8. Kim, K.J.; Sessler, A. Free-electron lasers: Present status and future prospects. *Science* **1990**, *250*, 88–93. [[CrossRef](#)] [[PubMed](#)]
9. Seo, Y.H.; Lee, W.H. Superradiant undulator radiation of periodic intense electron bunches in a cavity. *IEEE Trans. Plasma Sci.* **2010**, *38*, 2016–2020. [[CrossRef](#)]
10. Tan, P.; Huang, J.; Liu, K.; Xiong, Y.; Fan, M. Terahertz radiation sources based on free electron lasers and their applications. *Sci. China Inf. Sci.* **2012**, *55*, 1–15. [[CrossRef](#)]
11. Sikharin, S.; Tsugamura, Y.; Zen, H.; Kii, T.; Ohgaki, H. Development of compact TH-FEL system at Kyoto University. In Proceedings of the FEL Conference, Basel, Switzerland, 25–29 August 2014; pp. 501–504.
12. Kovalev, S.; Wang, Z.; Deinert, J.C.; Awari, N.; Chen, M.; Green, B.; Germanskiy, S.; Oliveira, T.V.A.G.; Lee, J.S.; Deac, A. Selective THz control of magnetic order: New opportunities from superradiant undulator sources. *J. Phys. D Appl. Phys.* **2018**, *51*, 114007. [[CrossRef](#)]
13. Kampfprath, T.; Sell, A.; Klatt, G.; Pashkin, A.; Mährlein, S.; Dekorsy, T.; Wolf, M.; Fiebig, M.; Leitenstorfer, A.; Huber, R. Coherent terahertz control of antiferromagnetic spin waves. *Nat. Photonics* **2011**, *5*, 31–34. [[CrossRef](#)]
14. Baierl, S.; Mentink, J.H.; Hohenleutner, M.; Braun, L.; Do, T.M.; Lange, C.; Sell, A.; Fiebig, M.; Woltersdorf, G.; Kampfprath, T.; et al. Terahertz-driven nonlinear spin response of antiferromagnetic nickel oxide. *Phys. Rev. Lett.* **2016**, *117*, 107201. [[CrossRef](#)] [[PubMed](#)]
15. Zen, H.; Suphakul, S.; Kii, T.; Ohgaki, H.; Kuroda, R.; Taira, Y. Development of photocathode drive laser system for RF guns in KU-FEL. In Proceedings of the FEL Conference, Basel, Switzerland, 25–29 August 2014; pp. 828–831.
16. Krainara, S.; Zen, H.; Suphakul, S.; Kii, T.; Ohgaki, H. THz coherent undulator radiation generated from compact accelerator based on photocathode rf gun. In Proceedings of the PASJ Conference, Sapporo, Japan, 1–3 August 2017; pp. 118–121.
17. Krainara, S.; Zen, H.; Suphakul, S.; Kii, T.; Ohgaki, H. Development of compact THz coherent undulator radiation source at Kyoto University. In Proceedings of the FEL Conference, Santa Fe, NM, USA, 20–25 August 2017; pp. 158–161.
18. Krainara, S.; Zen, H.; Shuya, C.; Kii, T.; Ohgaki, H. Study of the saturation of radiation energy caused by the space charge effect in a compact THz coherent radiation source. *J. Phys. Conf. Ser.* **2018**, *1067*, 032022. [[CrossRef](#)]
19. Pencoa, G.; Allaria, E.; Badano, L.; Cinquegrana, P.; Craievich, P.; Danailova, M.; Demidovich, A.; Ivanova, R.; Lutman, A.; Rumiza, L.; et al. Optimization of a high brightness photoinjector for a seeded FEL facility. *J. Instrum.* **2013**, *8*, P05015. [[CrossRef](#)]
20. Harkay, K.C.; Li, Y.; Nemeth, K.; Rosenberg, R.A.; White, M.; Spentzouris, L.K. Photocathode studies for ultra-low-emittance electron sources. In Proceedings of the PAC Conference, Vancouver, BC, Canada, 4–8 May 2009; pp. 458–460.
21. Togawa, K.; Shintake, T.; Inagaki, T.; Onoe, K.; Tanaka, T.; Baba, H.; Matsumoto, H. CeB6 electron gun for low-emittance injector. *Phys. Rev. ST Accel. Beams* **2007**, *10*, 020703. [[CrossRef](#)]
22. Akre, R.; Dowell, D.; Emma, P.; Frisch, J.; Gilevich, S.; Hays, G.; Hering, P.; Iverson, R.; Limborg-Deprey, C.; Loos, H.; et al. Commissioning the Linac Coherent Light Source injector. *Phys. Rev. ST Accel. Beams* **2008**, *11*, 030703. [[CrossRef](#)]
23. Beaudoin, B.L.; Thangaraj, J.C.T.; Edstrom, D., Jr.; Ruan, J.; Lumpkin, A.H.; Broemmelsiek, D.; Carlson, K.A.; Crawford, D.J.; Romanov, A.; Santucci, J.K.; et al. Longitudinal bunch shaping of picosecond high-charge MeV electron beams. *Phys. Plasmas* **2016**, *23*, 103107. [[CrossRef](#)]

24. Hyun, K.; Yim, C.M.; Parc, Y.W.; Park, J.H.; Ko, I.S.; Kim, C.; Park, J. Longitudinal laser pulse shaping for low-emittance electron-beam generation. *J. Korean Phys. Soc.* **2009**, *54*, 381–385. [[CrossRef](#)]
25. Yang, J.; Sakai, F.; Yanagida, T.; Yorozu, M.; Okada, Y.; Takasago, K.; Endo, A.; Yada, A.; Washio, M. Low-emittance electron-beam generation with laser pulse shaping in photocathode radio-frequency gun. *J. Appl. Phys.* **2002**, *92*, 1608. [[CrossRef](#)]
26. Kim, C.; Park, J.; Hyun, K.; Yim, C.M.; Parc, Y.W.; Ko, I.S. Laser pulse shaping for generation of low-emittance electron beam. In Proceedings of the FEL Conference, Gyeongju, Korea, 24–29 August 2008; pp. 278–281.
27. Zhou, F.; Brachmann, A.; Emma, P.; Gilevich, S.; Huang, Z. Impact of the laser spatial distribution on the LCLS photocathode gun operation. *Phys. Rev. ST Accel. Beams* **2012**, *15*, 090701. [[CrossRef](#)]
28. Li, W.W.; Huang, R.X.; He, Z.G.; Jia, Q.K.; Zhou, G.Q. Generation and measurement of sub-picosecond electron bunch in photocathode RF gun. In Proceedings of the IPAC Conference, Shanghai, China, 12–17 May 2013; pp. 372–374.
29. Miyajima, T.; Honda, Y.; Yamamoto, M.; Uchiyama, T.; Harada, K.; Shimada, M.; Takai, R.; Kume, T.; Nagahashi, S.; Obina, T.; et al. Low emittance electron beam transportation in compact ERL injector. In Proceedings of the IPAC Conference, Dresden, Germany, 15–20 June 2014; pp. 3104–3106.
30. Travier, C. An introduction to photo-injector design. *Nucl. Instrum. Methods A* **1994**, *340*, 26–39. [[CrossRef](#)]
31. Kim, K.J. RF and space-charge effects in laser-driven rf electron guns. *Nucl. Instrum. Methods A* **1989**, *275*, 201–218. [[CrossRef](#)]
32. Stupakov, G.; Huang, Z. Space charge effect in an accelerated beam. *Phys. Rev. ST Accel. Beams* **2008**, *11*, 014401. [[CrossRef](#)]
33. Van der Geer, S.B.; de Loos, M.J. General Particle Tracer: A 3D code for accelerator and beam line design. In Proceedings of the EPAC Conference, Barcelona, Spain, 10–14 June 1996; pp. 1245–1247.
34. Wang, X.J.; Chang, X. Femto-seconds kilo-ampere electron beam generation. *Nucl. Instrum. Methods A* **2003**, *507*, 310–313. [[CrossRef](#)]
35. Wang, X.J.; Ben-Zvi, I. Longitudinal emittance compensation in a photocathode RF gun injector. In Proceedings of the PAC Conference, Vancouver, BC, Canada, 12–16 May 1997; p. 6259326.
36. He, A.; Willeke, F.; Yu, L.H.; Yang, L.; Shaftan, T.; Wang, G.; Li, Y.; Hidaka, Y.; Qiang, J. Design of low energy bunch compressors with space charge effects. *Phys. Rev. ST Accel. Beams* **2015**, *18*, 014201. [[CrossRef](#)]
37. Byrd, J. Bunch Compressors. Presented at the Lecture of Short Bunches in Accelerators: USPAS, Boston, MA, USA, 21–25 June 2010.
38. Kan, K.; Yang, J.; Kondoh, T.; Norizawa, K.; Yoshida, Y. Effect of emittance and space-charge in femtosecond bunch compression. *Nucl. Instrum. Methods A* **2008**, *597*, 126–131. [[CrossRef](#)]
39. Krainara, S.; Zen, H.; Shuya, C.; Kii, T.; Ohgaki, H. Electron beam optimization of THz Coherent Undulator Radiation source at Kyoto University. **2018**, in preparation.
40. Zhou, F.; Bohler, D.; Ding, Y.; Gilevich, S.; Huang, Z.; Loos, H.; Ratner, D.; Vetter, S. *Characterizing and Optimization Photocathode Laser Distributions for Ultra-Low Emittance Electron Beam Operations*; SLAC-PUB-16436; U.S. Department of Energy, Office of Science: Berkeley, CA, USA, 2015.
41. Serafini, L. Improving the beam quality of RF guns by correction of RF and space-charge effects. *AIP Conf. Proc.* **1992**, *279*, 645.
42. Chen, C.H.; Hwang, C.S.; Lau, W.K.; Huang, N.; Lee, A.P.; Chou, M.C.; Huang, Y.C.; Chao, F.H.; Wu, J.; Cha, A. Preliminary design of THz FEL. Presented at the Lecture of FEL School, Hsinchu, Taiwan, 18–22 January 2016.
43. Bocek, D. Generation and Characterization of Superradiant Undulator Radiation. Ph.D. Thesis, Stanford University, Stanford, CA, USA, 1997.
44. Damminsek, K.; Rimjaem, S.; Thongbai, C.; Suphakul, S.; Ohgaki, H.; Zen, H. Electron beam properties from a compact seeded terahertz FEL amplifier at Kyoto University. In Proceedings of the FEL Conference, Daejeon, Korea, 23–28 August 2015; pp. 85–88.

